CHEMISTRY OF MATERIALS
Cite This: Chem. Mater. 2018, 30, 8804−8810
Article
pubs.acs.org/cm

Effect of Crystallinity on Li Adsorption in Polyethylene Oxide

Deya Das, Anand Chandrasekaran, Shruti Venkatram, and Rampi Ramprasad*

School of Materials Science and Engineering, Georgia Institute of Technology, 771 Ferst Drive NW, Atlanta, Georgia 30332, United States

Supporting Information

ABSTRACT: Despite their numerous benefits, the use of solid-polymer electrolytes, such as polyethylene oxide (PEO), in next-generation Li-ion batteries is constrained by their lower ionic conductivity. To overcome this bottleneck and design materials with higher conductivity, it is important to elucidate the underlying atomistic mechanisms of Li-ion adsorption in such materials. Here, we have performed a comprehensive statistical analysis of the interaction of Li and Li^+ at numerous locations in crystalline and amorphous PEO. Our in-depth analysis of the Li−O bonding environment using ab initio calculations reveals that Li/Li^+ can bind with more number of oxygen atoms in amorphous PEO compared to crystalline case. The maximum value of coordination number, that is, the number of oxygen atoms bonded with Li/Li^+ is 3 for crystalline PEO and 5 for amorphous PEO. This can be attributed to the access to more neighboring oxygen atoms in amorphous PEO. Binding energy calculations reveal that the interaction of Li and Li^+ significantly depends on the degree of crystallinity. Li/Li^+ adsorption is preferable in amorphous PEO and the average binding energy difference in amorphous and crystalline PEO is 3.36 eV for Li and 2 eV for Li^+ because of greater free volume and higher coordination number in amorphous PEO. While the crystalline regions of PEO are required to provide robustness, amorphous regions have been found to facilitate Li^+ ion adsorption providing higher coordination number and stronger binding energy.

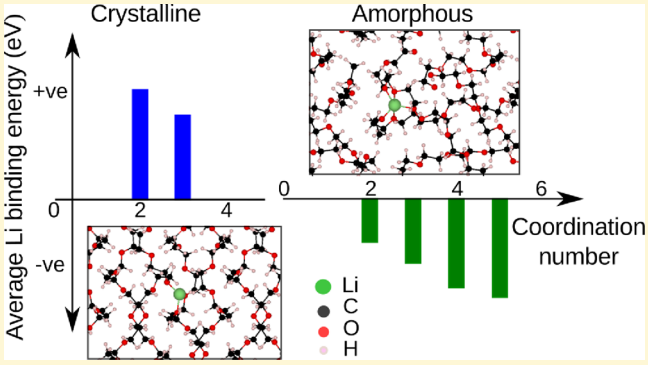

1. INTRODUCTION

As renewable energy sources are increasingly gaining traction as an alternative to scarce fossil fuels, exploratory research on energy storage devices, particularly Li-ion batteries (LIBs), has become prolific. LIBs have emerged as popular energy storage devices especially for use in hybrid vehicles and portable electronic devices, owing to their compact size and high energy density.[1−4] Commercial LIBs are composed of two electrodes, a liquid electrolyte, and a polymer separator. Usually, graphite serves as anode material, $LiCoO_2$ is used as cathode material, and binary solvent mixtures such as ethylene carbonate and dimethyl carbonate along with Li salt, lithium hexafluorophosphate ($LiPF_6$), are used as the basic standard electrolyte solutions for LIBs.[5,6] The electrodes are physically separated by a porous polymer membrane called a separator.[7] However, there have been safety issues surrounding electronics containing LIBs, viz., overheating leading to explosions. Major safety issues in LIBs concern the organic liquid electrolyte and the separator.[8,9] The organic liquid electrolyte undergoes decomposition reactions because of the high oxidation potentials of the cathodes and releases carbon dioxide, raising the pressure in a sealed LIB and eventually exploding.[9] The other problem is the polymer separator. To maximize the energy density, the separator is made as thin as possible.[10] If the separator is breached due to surface reactions, it causes a short circuit and triggers a process called thermal runaway.[11] The chemicals inside the battery heat up, causing further degradation of the separator eventually leading to an explosion or a fire.

To safely utilize a high-performing LIB, a few alternatives have been suggested, one of which is replacing the liquid electrolyte with a suitable solid polymer electrolyte (SPE).[12,13] SPEs offer several advantages over conventional liquid electrolytes, viz., low flammability, good processability, and no leakage issues. SPEs also eliminate the need for a separator,[14] thereby decreasing the chances of an accident. A promising SPE candidate should have high Li-ion conductivity,[15] a low glass transition temperature (both of which depend on the degree of crystallinity of the polymer[16]), as well as an electrochemical stability window larger than the difference between the electrochemical potentials of cathode and anode.[9] However, pure SPE systems have conductivities limited to $\sim 10^{-5}$ S/cm at room temperature[9,17] which is a few orders of magnitudes lower than their ionic liquid counterparts.

Polyethylene oxide (PEO) was the first solid electrolyte system developed in 1973[18] and is still the leading choice for a SPE. The morphology of PEO electrolyte in Li ion battery is a mixed phase between crystalline and amorphous regions.[15]

Received: August 11, 2018
Revised: December 1, 2018
Published: December 2, 2018

DOI: 10.1021/acs.chemmater.8b03434
Chem. Mater. 2018, 30, 8804−8810

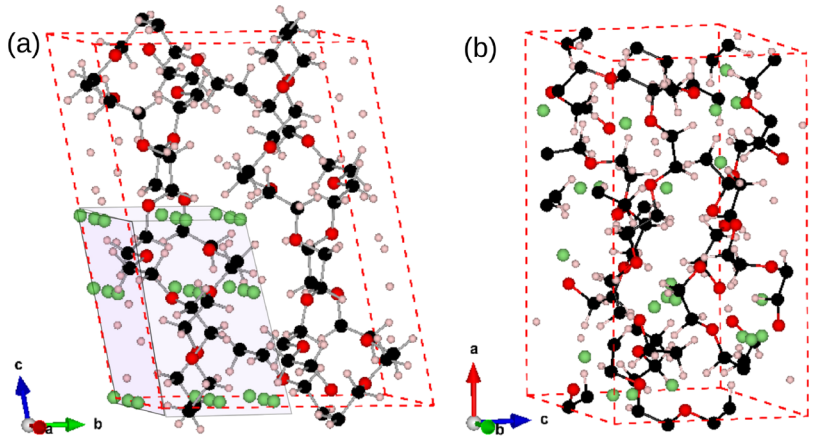

Figure 1. (a) Structure of PEO crystal with 27 chosen initial positions of neutral Li atom/Li^+ ion where black, red, pink, and green spheres denote C, O, H, and Li atoms, respectively. Li positions are chosen only in one-quarter of unit cell to exploit the inherent symmetry of the unit cell. (b) 20 minimum energy positions out of 1000 initial positions for Li atom/Li^+ ion in amorphous PEO structure.

Molecular dynamics (MD) studies have established that the Li^+ ion forms complexes with the O atoms of PEO and travels via the segmental motion of the PEO molecule.[19,20] The range of segmental motion depends on the amorphicity of the polymer; greater amorphicity leads to larger free volume leading to greater chain flexibility and motion. Although most studies on PEO have tried to maximize amorphicity, a few studies[21,22] have shown that specific PEO metal alkali oxide compositions form cylindrical tunnels of PEO helices through which Li^+ ions travel unhindered. Further studies have found that crystalline PEO shows higher conductivity only for specific cases, while, in general, the symmetry of crystalline structures leads to a greater energy barrier for the Li^+ ion to cross due to the greater steric hindrance caused by O atoms.[23] However, a systematic understanding of the effect of crystallinity on Li ion adsorption is still lacking.

Here, we study both crystalline and amorphous PEO structures to understand how crystallinity affects the adsorption of neutral Li atom and Li^+ ion using density functional theory (DFT) computations. Because Li binding to the host is the first step and a prelude to Li migration, we focus our efforts in this study to just Li binding to a PEO host. Our study is comprehensive, in which the statistical variation of the tendency of Li (in neutral and charged states) to bind to a variety of sites in prototypical crystalline and amorphous PEO has been considered. We find that the Li atom/Li^+ ion binds with neighboring O atoms. The maximum values of the coordination number, the number of oxygen atoms bonded with Li/Li^+, are higher in amorphous PEO compared to crystalline PEO. This can be attributed to coiled PEO chains and more O atoms in the vicinity of Li atom/Li^+ ion in amorphous PEO. Our study reveals that the Li^+ ion clearly prefers to reside in the amorphous phase of PEO rather than in the crystalline phase (in a statistical sense). Therefore, amorphous regions of PEO have been found to be the perfect host for Li^+ ion, providing high coordination number and binding energy that can be tailored based on the electrochemical potential of electrodes.

2. METHODOLOGY

The calculations were performed using DFT as implemented in the Vienna Ab initio Simulation Package (VASP).[24,25] The electron−ion interactions were captured using all-electron projector augmented wave potentials,[26] and the electronic exchange correlations were approximated using the Perdew−Burke−Ernzerhof generalized gradient approximation.[27,28] Geometry optimizations were performed using the conjugate gradient scheme, until the forces on each atom were of the order of 10^{-3} eV/Å. The Brillouin zone was sampled by $5 \times 3 \times 2$ and $1 \times 2 \times 1$ k-grids using a Monkhorst−Pack scheme for crystalline and amorphous PEO, respectively. The kinetic energy cutoff for the plane wave was set to 400 eV to ensure the accuracy of the calculations. Gaussian smearing with smearing width of 0.1 eV was used for electronic structure calculations. van der Waals (vdW) dispersion interactions were included via the vdW-DF2 non-local density functional simulations.[29,30] To generate amorphous PEO structures, classical MD simulations were performed using LAMMPS package (http://lammps.sandia.gov).[31] The Nose−Hoover thermostat and barostat were utilized in the *NVT* and *NPT* simulations, respectively. The all-atom optimized potentials for liquid simulations force field[32,33] was employed to simulate all inter- and intramolecular interactions. All nonbonded interactions beyond a 9.5 Å cutoff were calculated using particle−particle−mesh Ewald summation. Velocity Verlet integrator with a 2 fs time step has been employed to update the new position and velocities of the atoms.

The binding energy of neutral Li atom/Li^+ ion to PEO was calculated using the following equation[34,35]

$$E_b^q(\mu) = E^q_{\mathrm{PEO+Li/Li^+}} - E_{\mathrm{PEO}} - E_{\mathrm{Li}} + q(\mu + E_{\mathrm{VBM}} + \Delta V) + E_{\mathrm{corr}} \quad (1)$$

where $E^q_{\mathrm{PEO+Li/Li^+}}$ and E_{PEO} are the total energies, respectively, of crystalline or amorphous PEO with neutral Li atom/Li^+ ion and pure crystalline or amorphous PEO. E_{Li} is the Li chemical potential of Li, taken to be the energy per atom of crystalline bulk Li which occurs as a body centered cubic structure. μ is the electronic chemical potential, which varies from valence band maximum (VBM) to conduction band minimum (CBM) of the crystalline/amorphous PEO depending on the difference between the electrochemical potential of electrodes. However, the binding energy of neutral Li (corresponding to $q = 0$) does not depend on μ, and eq 1 would consist of the first three terms only. In the case of Li^+ (corresponding to $q = 1$), there are two additional correction terms, as shown in eq 1. ΔV is

DOI: 10.1021/acs.chemmater.8b03434
Chem. Mater. 2018, 30, 8804−8810

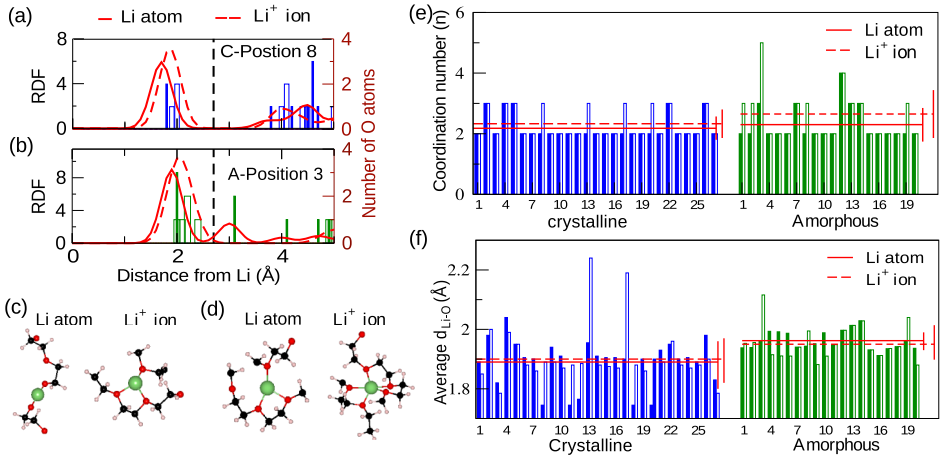

Figure 2. Plot of RDF of O atoms for (a) position 8 and (b) position 3 in crystalline and amorphous PEO, respectively. The number of O atoms located at different distances from Li atom/Li^+ ion is also plotted in these graphs as marked in right hand side *y*-axis, where solid and open bars correspond to neutral Li and Li^+ ion adsorption, respectively. Blue and green colors denote crystalline and amorphous PEO, respectively. The total number of O atoms under the first peak of RDF plot, that is, total number of O atoms within the distance of 2.7 Å (marked by black dashed line) from Li atom/Li^+ ion, is considered as coordination number (n). (c,d) Local structures near neutral Li atom/Li^+ ion are shown for the cases considered in (a,b). (e) Plot of coordination numbers (n) for 27 and 20 different Li atom/Li^+ ion positions in crystalline and amorphous PEO, respectively. Solid and open bars side by side denote neutral Li atom and Li^+ ions, respectively, for a particular position. Average n values for all Li atom (Li^+ ion) positions are shown by solid (dashed) red line with standard deviation for both crystalline and amorphous cases. (f) Plot of average bond length (d_{Li-O}) between Li and O atoms over n cases for 27 and 20 different Li atom/Li^+ ion positions in crystalline and amorphous PEO, respectively, where solid and open bars denote neutral Li atom and Li^+ ion, similar to (e). Total average over all Li atom (Li^+ ion) positions are shown by solid (dashed) red line with standard deviation for both crystalline and amorphous cases.

the correction term to appropriately line up the energy zero of the supercells with and without the defect. ΔV was determined by calculating the energy difference of the core oxygen 1s orbitals between two cases. E_{corr} represents spurious electrostatic interactions of charged defects due to periodicity and finite supercell sizes. We have considered only the first-order monopole correction.[36,37] According to the definition of binding energy as prescribed by eq 1, more negative values indicate that the adsorption of neutral Li atom/Li^+ ion is energetically more favorable. Li should bind in the electrolyte with an optimum binding energy. The binding energy should be strong enough to bind Li; however, it should not be very high to inhibit Li diffusion during charging/discharging. The lower bound of this optimal window is defined by the energy of bulk Li (how much Li prefers to bind in PEO than Li clustering), while the upper bound is set by the voltage difference between the electrodes and the energy barrier for Li diffusion, which governs Li shuttling between electrodes during charging/discharging.

3. RESULTS AND DISCUSSION

3.1. Structural Details of Crystalline and Amorphous PEO. To understand the atomistic mechanism of Li^+ ion adsorption in PEO, we studied crystalline and amorphous PEO separately. The most stable crystal structure of PEO[38] with four (7/2) helical chains in a unit cell (space group $P_2 1/a\text{-}C_{2h}^5$) was considered (Figure 1a). The optimized lattice parameters are in good agreement with previously reported studies,[38] as mentioned in Table S1 in Supporting Information.

Amorphous PEO structures were generated via a "melt and quench"[39,40] procedure using a classical MD simulation. The detail of this process is described in Supporting Information. The resulting amorphous PEO structure, shown in Figure 1b, has a density of 1.08 g/cm^3, which is close to the reported value of 1.12 g/cm^3.[41,42] The experimentally reported density of crystalline PEO is 1.24 g/cm^3,[41,42] implying that amorphous PEO has more free volume compared to crystalline PEO. The radial distribution function (RDF) of amorphous PEO shown in Figure S1b exhibits no long range order, consistent with the amorphicity of this structure.

3.2. Structural Changes after Li Atom/Li^+ Ion Adsorption. Although Li^+ ion shuttles through the electrolyte during charging/discharging of a LIB, adsorption of neutral Li atom might also occur depending on the electrochemical potential of electrodes. It is important to understand the difference between the adsorption of a Li^+ ion and a neutral Li atom. Therefore, we have studied the adsorption of a neutral Li atom and a Li^+ ion in crystalline and amorphous PEO to understand how such factors would alter the physical and electronic structures.

To capture the statistical variation across different local environments, 27 inequivalent positions were chosen in crystalline PEO by considering Li placements in a 3 × 3 × 3 spatial grid in one-quarter of the crystalline PEO unit cell. The reduced size was chosen to exploit the inherent symmetry of the unit cell as shown in Figure 1a. In amorphous PEO, the chains are randomly coiled and lack structural symmetry. Therefore, we do not have the advantage of using structural symmetry while choosing the positions for Li atom/Li^+ ion adsorption. Thus, the entire cell of the amorphous PEO structure was scanned by single point calculations with 10 × 10 × 10 grid points (i.e., 1000 different locations for Li in the amorphous PEO host). The 20 lowest energy positions were selected among the 1000 positions for further calculations (shown in Figure 1b). Although, the starting positions of both neutral Li and Li^+ ion are the same, the positions of Li and the local structures around Li and Li^+ ion are different postrelaxation.

Neutral Li atom or Li^+ ion binds with oxygen atoms in PEO. The changes in local structure around them were investigated by calculating Li−O RDF.[43] In Figure 2a,b, Li−O RDF curves

DOI: 10.1021/acs.chemmater.8b03434
Chem. Mater. 2018, 30, 8804−8810

(in red) have been plotted for a random position in crystalline (position 8) and amorphous PEO (position 3). Figure 2a,b also shows the number of oxygen atoms (right hand side *y*-axis) as a function of distance from Li, where solid and open bars denote the adsorption of neutral Li atom and Li^+ ion, respectively, and blue (Figure 2a) and green bars (Figure 2b) denote crystalline and amorphous PEO, respectively. The first peak in the RDF plot denotes the closest oxygen atoms bonded with Li atom/Li^+ ion, and the number of bonded oxygen atoms (denoted by bars under the first peak of RDF plot) is the coordination number (n).[43] These n O atoms are found to be at less than 2.7 Å from Li atom/Li^+ ion and this bond-length limit, shown by black dashed line in Figure 2a,b, is in good agreement with a previous report.[44]

For the Li atom/Li^+ ion position-8 in crystalline PEO (Figure 2a), n is 2 for neutral Li adsorption and is 3 for Li^+ ion adsorption. The local structures near neutral Li atom and Li^+ ion corresponding to this position are shown in Figure 2c. The O atom in one of the PEO chains, situated far from neutral Li, comes closer to Li^+ ion and binds with it, thereby increasing coordination number. In Figure 2b, corresponding to Li atom/Li^+ ion position-3 in amorphous PEO, n is 3 for Li atom and it increases to 5 for the adsorption of Li^+ ion. The corresponding local structures are shown in Figure 2d.

In Figure 2e, the coordination numbers (n) are plotted for all 27 and 20 positions of Li atom/Li^+ ion in crystalline and amorphous PEO, respectively. For a particular position of Li, solid and open bars, side by side, correspond to neutral Li atom and Li^+ ion adsorption, respectively. The average n value for all the positions separately in crystalline and amorphous PEO is marked by solid (dashed) red lines for Li atom (Li^+ ion) adsorption with standard deviation shown by a red solid vertical line. We find that, in crystalline PEO, Li atom/Li^+ ion generally binds with two oxygen atoms (n = 2), which is in good agreement with previous studies.[43,45] However, there are few cases where the coordination number is 3. The average coordination number is 2.18 and 2.33 for neutral Li and Li^+ ion, respectively. In amorphous PEO, the most preferable coordination number is 2 and for few cases, it becomes higher, ranging from 3 to 5. The average coordination number is 2.30 for neutral Li and 2.65 for Li^+ ion. However, by comparing the standard deviation in crystalline and amorphous cases, the coordination numbers for both cases turn out to be similar. The maximum values of coordination numbers, on the other hand, are slightly higher in amorphous PEO compared to those of the crystalline case because the Li atom/Li^+ ion has access to bind with more number of oxygen atoms due to the higher level of configurational freedom available in the amorphous phase.

The average bond length (d_{Li-O}) between Li and n number of O atoms corresponding to a particular Li position is plotted for all 27 positions in crystalline PEO and 20 positions for amorphous PEO in Figure 2f. Solid and open bars, side by side, denote neutral Li atom and Li^+ ion, respectively, for a particular position of neutral Li atom/Li^+ ion, similar to Figure 2e. The total average over all the cases separately in crystalline and amorphous PEO is shown by solid (dashed) red line for neutral Li (Li^+ ion) with standard deviation marked by red solid vertical line. Neutral Li atom binds with neighboring oxygen atoms having a Li−O distance of 1.89 Å in crystalline PEO and it remains almost the same for the adsorption of Li^+ ion, which is in good agreement with previous reports.[46] However, in amorphous PEO, the Li−O bond length slightly increases to 1.96 Å for both neutral Li atom/Li^+ ion because there is more free volume in the amorphous case. From Figure 2e,f, we find that, in general, a higher coordination number leads to higher average d_{Li-O} for both crystalline and amorphous PEO irrespective of the charge states of Li. We also plotted the RDF considering all of the lithium species as shown in Figure S2 in Supporting Information by solid and dashed red lines for Li atom and Li^+ ion, respectively. The peaks of RDF are obtained for Li atom at 1.8 Å and for Li ion at 1.9 Å in crystalline PEO, whereas these two numbers are 1.8 and 2 Å, respectively in amorphous PEO. In the same plot, the number of oxygen atoms from Li atom and Li^+ ion is plotted by solid and open bars, respectively, and blue and green colors denote crystalline and amorphous PEO, respectively. It shows that in crystalline PEO, the average coordination number for Li atom adsorption is 2.18 and for Li ion adsorption is 2.33. In amorphous PEO, the average coordination number for Li atom is 2.30 and for Li ion is 2.65. These coordination numbers are exactly same and the average Li−O distance values are almost same as we obtained from Figure 2e,f, denoting higher average coordination number and higher average Li−O distances in amorphous PEO.

3.3. Electronic Structure. Next, the electronic structures were investigated for crystalline and amorphous PEO with adsorbed neutral Li and Li^+ ion by analyzing the electronic density of states as shown in Figure S3 in Supporting Information. Crystalline PEO is an insulator with a 5 eV band gap, which reduces to 4.27 eV for amorphous PEO. Experimental studies for semicrystalline polymer PEO films reported the band gap to be 4.62 eV.[47,48] In the presence of neutral Li, defect states appear close to both VBM and CBM as marked by red circles in Figure S3. The extra electron coming from the Li 2s orbital occupies the defect state close to the CBM, which shifts the Fermi level higher as shown in Figure S3. On removal of this electron, that is, in the case of the Li^+ case, the defect states close to CBM become empty as marked by red circles and the Fermi level shifts back to the same position as in Li-free crystalline/amorphous PEO.

3.4. Binding Energy and Charge Transition Level. The binding energies corresponding to adsorption of Li atom/Li^+ ion for 27 and 20 positions in crystalline and amorphous PEO, respectively, were calculated using eq 1, as mentioned in the Methodology section. The binding energies for both neutral Li (solid red line) and Li^+ ion (dashed red line) are plotted for position 1 in amorphous PEO in Figure 3a as a function of electronic chemical potential (μ), where μ is referenced to the VBM. The binding energy for Li^+ ion is −1.63 eV at VBM corresponding to μ = 0 and it changes linearly as a function of μ. On the other hand, for neutral Li atom adsorption, the binding energy is 0.73 eV, which is independent of μ. Binding energy lines, corresponding to q = 0 and 1, cross each other at a certain value of μ (2.37 eV), defined as charge transition level E_T (marked in green line). According to this plot, as μ varies from VBM to CBM of the crystalline/amorphous PEO depending on the electrochemical potential of electrodes, adsorption of Li^+ ion is preferable till μ reaches E_T, and after that, neutral Li adsorption becomes preferable. The charge transition levels for 27 positions in crystalline PEO and 20 positions in amorphous PEO are marked by blue and green lines, respectively, between VBM and CBM in Figure 3b. The values of E_T span a wide range in crystalline PEO from 1.44 to 4.30 eV above the VBM, while the amorphous PEO range is smaller from 1.52 eV to 2.62 eV.

DOI: 10.1021/acs.chemmater.8b03434
Chem. Mater. 2018, 30, 8804−8810

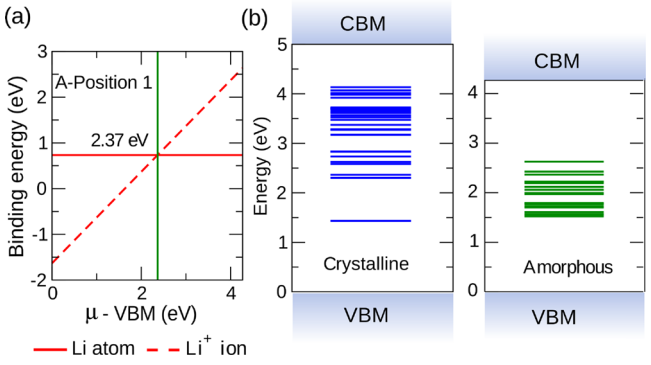

Figure 3. (a) Binding energies of neutral Li and Li^+ ion as a function of electronic chemical potential μ, where μ is referenced to the VBM for Li-position 1 in amorphous case. This plot denotes that adsorption of Li^+ ion is preferable till μ reaches charge transition level E_T marked in green solid line, and after that, neutral Li adsorption becomes preferable. (b) Values of charge transition levels for 27 and 20 Li positions in crystalline and amorphous cases are marked by blue and green lines, respectively, between the band edges.

The binding energies are plotted for both crystalline and amorphous PEO for the adsorption of neutral Li in Figure 4a and Li^+ ion in Figure 4b, respectively. In Figure 4b, for comparison, the binding energy values are considered for a special case ($\mu = 0$), which shows the strongest binding energy limit. The average binding energies for all the positions of Li atom (Li^+ ion) are shown by solid (dashed) red lines for both crystalline and amorphous cases with standard deviation, marked by solid red vertical line. We find that crystalline PEO shows poor binding of Li atom/Li^+ ion (positive binding energy). It is reported that crystalline phases may serve as useful salt reservoirs in the systems,[45] indicating less dissociation of Li-salts due to poor adsorption of Li^+ ion. The binding energy for amorphous PEO is negative, indicating that it is energetically favorable, owing to greater free volume available in amorphous PEO. The average binding energy difference between amorphous and crystalline PEO is 3.36 eV for Li atom and 2 eV for Li^+ ion. Kumar et al.[49] reported that Li salt induces a crystalline to amorphous transition in PEO, leading to an enhancement in conductivity. This indirectly supports the notion that Li^+ ions are more soluble (i.e., bind better) in amorphous PEO.

To understand the effect of coordination number on binding energy, the average values of binding energies for all the positions corresponding to a certain coordination number are plotted separately for crystalline and amorphous cases for both charge states of Li in Figure 4c. In all four cases, higher coordination number leads to stronger binding energy of Li atom/Li^+ ion. This is expected because more energy would be required to remove a Li if it is bonded with more number of O atoms. From Figure 4c, it can be seen that the Li^+ ion binds with more number of oxygen atoms in amorphous PEO with stronger binding energy.

4. SUMMARY

The low ionic conductivity supported by PEO is one of the main challenges for the development of PEO-based SPEs for Li ion batteries. Li ion conductivity in SPEs depends on the Li ion adsorption and diffusivity, which is sensitive to the SPE degree of crystallinity. To understand the effects of crystallinity, we have chosen PEO as a model system and studied the structural changes and binding energies due to neutral Li and Li^+ ion adsorption in both crystalline and amorphous PEO. Numerous Li positions within these structures were considered to provide an understanding of the statistical variations in binding modes and tendencies across different local environments. Table 1 captures the statistics underlying the key parameters (Li coordination number, average Li−O bond lengths, and Li binding energies) obtained in this study for crystalline and amorphous models of PEO. The corresponding standard deviations are also provided for each parameter.

Table 1. Average Coordination Number (n), Average Li−O Bond Length (d_{Li-O}), and Average Binding Energy (E_b) Values over 27 and 20 Positions of Li Atom/Li^+ Ion in Crystalline and Amorphous PEO, Respectively with Standard Deviation

	crystalline		amorphous	
	Li atom	Li^+ ion	Li atom	Li^+ ion
n	2.18 ± 0.39	2.33 ± 0.47	2.3 ± 0.56	2.65 ± 0.79
d_{Li-O} (Å)	1.89 ± 0.08	1.90 ± 0.07	1.96 ± 0.03	1.95 ± 0.06
E_b (eV)	4.04 ± 0.75	0.72 ± 0.38	0.68 ± 0.15	−1.27 ± 0.33

The results obtained here constitute a stepping stone toward establishing a baseline for comparing other potential SPE materials with PEO, an ubiquitous SPE. For instance, the binding energy of Li^+ ion in other polymers can be compared to that of amorphous PEO to decide whether those polymers are suitable SPE candidates. Key findings of this study include:

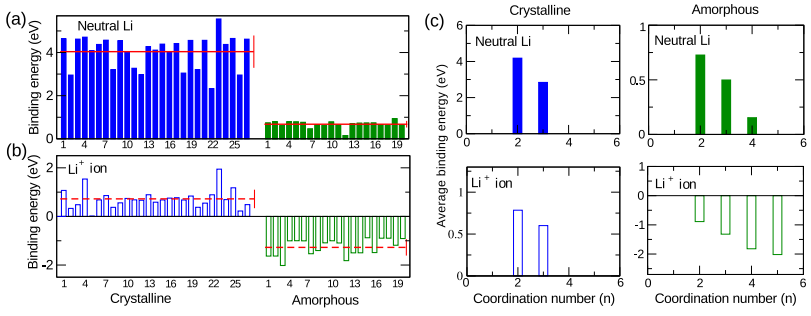

Figure 4. Plot of the binding energies for the adsorption of (a) Li atom and (b) Li^+ ion (corresponding to $\mu = 0$) for all 27 positions in crystalline and 20 positions in amorphous PEO structure. The average values of binding energy are denoted by red solid (dashed) lines for neutral Li (Li^+ ion) adsorption with standard deviation marked by red solid vertical line. (c) Average binding energy of neutral Li and Li^+ ion as a function of coordination number (n) in crystalline and amorphous PEO. Solid and open bars denote the adsorption of neutral Li and Li^+ ion, respectively.

DOI: 10.1021/acs.chemmater.8b03434
Chem. Mater. 2018, 30, 8804−8810

- Li atom/Li^+ ion binds with neighboring oxygen atoms in PEO. The O coordination number of Li in PEO (suitably defined as described in this manuscript) is similar in crystalline and amorphous PEO, considering the standard deviation for both cases. The maximum values of coordination numbers, however, are greater for amorphous PEO compared to the crystalline case due to the accessibility of more O atoms.
- The Li−O bond length is marginally greater in amorphous PEO because the amorphous structure has more free volume.
- The binding energy calculations show that binding tendencies of Li atom/Li^+ ion significantly depend on the degree of crystallinity. Li^+ ion adsorption is found to be energetically preferable only in amorphous PEO.
- Binding energy becomes stronger as the O coordination number of Li increases in both the crystalline and amorphous PEO phases.

Our comprehensive study finds that amorphous regions of PEO facilitate the binding of Li^+ ion providing negative binding energy due to larger free volume and high coordination number. These results correlate well with the reported result that Li^+ ions are more soluble in amorphous PEO. Besides providing fundamental understanding, the structure-binding energy data compiled in this study can contribute toward data-driven estimates[50−57] of Li interactions with polymers.

■ ASSOCIATED CONTENT

Supporting Information

The Supporting Information is available free of charge on the ACS Publications website at DOI: 10.1021/acs.chemmater.8b03434.

Structural details of crystalline PEO; process of amorphous PEO generation, Li−O radial distribution function for all Li positions, and the electronic structure and density of crystalline and amorphous PEO with adsorbed Li atom/Li^+ ion (PDF)

■ AUTHOR INFORMATION

Corresponding Author

*E-mail: rampi.ramprasad@mse.gatech.edu.

ORCID

Deya Das: 0000-0003-3860-9674

Rampi Ramprasad: 0000-0003-4630-1565

Notes

The authors declare no competing financial interest.

■ ACKNOWLEDGMENTS

The authors acknowledge support of this work by Toyota Research Institute through the Accelerated Materials Design and Discovery program. Computational support was provided by the Extreme Science and Engineering Discovery Environment (XSEDE) and Georgia Tech supercomputing facilities. The authors acknowledge Dr. L. Chen for useful discussions.

■ REFERENCES

(1) Kang, K.; Meng, Y. S.; Bréger, J.; Grey, C. P.; Ceder, G. Electrodes with High Power and High Capacity for Rechargeable Lithium Batteries. *Science* **2006**, *311*, 977−980.

(2) Kang, B.; Ceder, G. Battery Materials for Ultrafast Charging and Discharging. *Nature* **2009**, *458*, 190−193.

(3) Armand, M.; Grugeon, S.; Vezin, H.; Laruelle, S.; Ribière, P.; Poizot, P.; Tarascon, J.-M. Conjugated Dicarboxylate Anodes for Li-ion Batteries. *Nat. Mater.* **2009**, *8*, 120−125.

(4) Morcrette, M.; Rozier, P.; Dupont, L.; Mugnier, E.; Sannier, L.; Galy, J.; Tarascon, J.-M. A Reversible Copper Extrusion-Insertion Electrode for Rechargeable Li Batteries. *Nat. Mater.* **2003**, *2*, 755−761.

(5) Guyomard, D.; Tarascon, J. M. Li Metal-Free Rechargeable $LiMn_2O_4$/Carbon Cells: Their Understanding and Optimization. *J. Electrochem. Soc.* **1992**, *139*, 937−948.

(6) Tarascon, J. M.; McKinnon, W. R.; Coowar, F.; Bowmer, T. N.; Amatucci, G.; Guyomard, D. Synthesis Conditions and Oxygen Stoichiometry Effects on Li Insertion into the Spinel $LiMn_2O_4$. *J. Electrochem. Soc.* **1994**, *141*, 1421−1431.

(7) Zhang, S. S. A Review on the Separators of Liquid Electrolyte Li-ion Batteries. *J. Power Sources* **2007**, *164*, 351−364.

(8) Balakrishnan, P. G.; Ramesh, R.; Prem Kumar, T. Safety Mechanisms in Lithium-ion Batteries. *J. Power Sources* **2006**, *155*, 401−414.

(9) Goodenough, J. B.; Kim, Y. Challenges for Rechargeable Li Batteries. *Chem. Mater.* **2010**, *22*, 587−603.

(10) Orendorff, C. J. The role of Separators in Lithium-ion Cell Safety. *Electrochem. Soc. Interface* **2012**, *21*, 61−65.

(11) Wang, Q.; Ping, P.; Zhao, X.; Chu, G.; Sun, J.; Chen, C. Thermal Runaway Caused Fire and Explosion of Lithium Ion battery. *J. Power Sources* **2012**, *208*, 210−224.

(12) Meyer, W. H. Polymer Electrolytes for Lithium-Ion Batteries. *Adv. Mater.* **1999**, *10*, 439−448.

(13) Scrosati, B.; Vincent, C. A. Polymer Electrolytes: The Key to Lithium Polymer Batteries. *MRS Bull.* **2011**, *25*, 28−30.

(14) Kim, J. G.; Son, B.; Mukherjee, S.; Schuppert, N.; Bates, A.; Kwon, O.; Choi, M. J.; Chung, H. Y.; Park, S. A Review of Lithium and Non-lithium Based Solid State Batteries. *J. Power Sources* **2015**, *282*, 299−322.

(15) Xue, Z.; He, D.; Xie, X. Poly(ethylene oxide)-based Electrolytes for Lithium-ion Batteries. *J. Mater. Chem. A* **2015**, *3*, 19218−19253.

(16) Yue, L.; Ma, J.; Zhang, J.; Zhao, J.; Dong, S.; Liu, Z.; Cui, G.; Chen, L. All Solid-state Polymer Electrolytes for High-performance Lithium Ion Batteries. *Energy Storage Mater.* **2016**, *5*, 139−164.

(17) Tarascon, J.-M.; Armand, M. Issues and Challenges Facing Rechargeable Lithium Batteries. *Nature* **2001**, *414*, 359−367.

(18) Fenton, D. E.; Parker, J. M.; Wright, P. V. Complexes of Alkali Metal Ions with Poly(ethylene oxide). *Polymer* **1973**, *14*, 589.

(19) Müller-Plathe, F.; van Gunsteren, W. F. Computer Simulation of a Polymer Electrolyte: Lithium Iodide in Amorphous Poly(ethylene oxide). *J. Chem. Phys.* **1995**, *103*, 4745−4756.

(20) Cowie, J. M. G.; Spence, G. H. Novel Single Ion, Comb-branched Polymer Electrolytes. *Solid State Ionics* **1999**, *123*, 233−242.

(21) Gadjourova, Z.; Andreev, Y. G.; Tunstall, D. P.; Bruce, P. G. Ionic Conductivity in Crystalline Polymer Electrolytes. *Nature* **2001**, *412*, 520−523.

(22) Fu, X.-B.; Yang, G.; Wu, J.-Z.; Wang, J.-C.; Chen, Q.; Yao, Y.-F. Fast Lithium-Ion Transportation in Crystalline Polymer Electrolytes. *ChemPhysChem* **2017**, *19*, 45−50.

(23) Xue, S.; Liu, Y.; Li, Y.; Teeters, D.; Crunkleton, D. W.; Wang, S. Diffusion of Lithium Ions in Amorphous and Crystalline Poly-(ethylene oxide)$_3$:$LiCF_3SO_3$ Polymer Electrolytes. *Electrochim. Acta* **2017**, *235*, 122−128.

(24) Kresse, G.; Hafner, J. Ab initio molecular dynamics for liquid metals. *Phys. Rev. B: Condens. Matter Mater. Phys.* **1993**, *47*, 558−561.

(25) Kresse, G.; Joubert, D. From Ultrasoft Pseudopotentials to the Projector Augmented-wave Method. *Phys. Rev. B: Condens. Matter Mater. Phys.* **1999**, *59*, 1758−1775.

(26) Blöchl, P. E. Projector Augmented-wave Method. *Phys. Rev. B: Condens. Matter Mater. Phys.* **1994**, *50*, 17953−17979.

(27) Perdew, J. P.; Burke, K.; Ernzerhof, M. Generalized Gradient Approximation Made Simple. *Phys. Rev. Lett.* **1996**, *77*, 3865−3868.

DOI: 10.1021/acs.chemmater.8b03434
Chem. Mater. 2018, 30, 8804−8810

(28) Kresse, G.; Furthmüller, J. Efficiency of Ab-initio Total Energy Calculations for Metals and Semiconductors Using a Plane-wave Basis Set. *Comput. Mater. Sci.* **1996**, *6*, 15−50.
(29) Lee, K.; Murray, E. D.; Kong, L.; Lundqvist, B. I.; Langreth, D. C. Higher-accuracy van der Waals Density Functional. *Phys. Rev. B: Condens. Matter Mater. Phys.* **2010**, *82*, No. 081101(R).
(30) Klimeš, J.; Bowler, D. R.; Michaelides, A. Chemical Accuracy for the van der Waals Density Functional. *J. Phys.: Condens. Matter* **2010**, *22*, 022201.
(31) Plimpton, S. Fast Parallel Algorithms for Short-Range Molecular Dynamics. *J. Comput. Phys.* **1995**, *117*, 1−19.
(32) Jorgensen, W. L.; Maxwell, D. S.; Tirado-Rives, J. Development and Testing of the OPLS All-Atom Force Field on Conformational Energetics and Properties of Organic Liquids. *J. Am. Chem. Soc.* **1996**, *118*, 11225−11236.
(33) Siu, S. W. I.; Pluhackova, K.; Böckmann, R. A. Optimization of the OPLS-AA Force Field for Long Hydrocarbons. *J. Chem. Theory Comput.* **2012**, *8*, 1459−1470.
(34) Ramprasad, R.; Zhu, H.; Rinke, P.; Scheffler, M. New Perspective on Formation Energies and Energy Levels of Point Defects in Nonmetals. *Phys. Rev. Lett.* **2012**, *108*, 066404.
(35) Janotti, A.; Van de Walle, C. G. Native Point Defects in ZnO. *Phys. Rev. B: Condens. Matter Mater. Phys.* **2007**, *76*, 165202.
(36) Makov, G.; Payne, M. C. Periodic boundary conditions in ab initio calculations. *Phys. Rev. B: Condens. Matter Mater. Phys.* **1995**, *51*, 4014−4022.
(37) Neugebauer, J.; Scheffler, M. Adsorbate-substrate and Adsorbate-adsorbate Interactions of Na and K Adlayers on Al(111). *Phys. Rev. B: Condens. Matter Mater. Phys.* **1992**, *46*, 16067−16080.
(38) Takahashi, Y.; Tadokoro, H. Structural Studies of Polyethers, $(-(CH_2)_m-O-)_n$. X. Crystal Structure of Poly(ethylene oxide). *Macromolecules* **1973**, *6*, 672−675.
(39) Chen, L.; Huan, T. D.; Ramprasad, R. Electronic Structure of Polyethylene: Role of Chemical, Morphological and Interfacial Complexit. *Sci. Rep.* **2017**, *7*, 6128.
(40) Webb, M. A.; Jung, Y.; Pesko, D. M.; Savoie, B. M.; Yamamoto, U.; Coates, G. W.; Balsara, N. P.; Wang, Z.-G.; Miller, T. F. Systematic Computational and Experimental Investigation of Lithium-Ion Transport Mechanisms in Polyester-Based Polymer Electrolytes. *ACS Cent. Sci.* **2015**, *1*, 198−205.
(41) Wunderlich, B. *Crystal Structure, Morphology and Defects*; Academic Press: New York, 1973; Vol. *1*, pp 388−389.
(42) Sun, L.; Zhu, L.; Rong, L.; Hsiao, B. S. Tailor-Made Onionlike Stereocomplex Crystals in Incompatible, Enantiomeric, Polylactide-Containing Block Copolymer Blends. *Angew. Chem., Int. Ed.* **2006**, *45*, 7373−7376.
(43) Johansson, P. First principles modelling of amorphous polymer electrolytes: Li^+-PEO, Li^+-PEI, and Li^+-PES complexes. *Polymer* **2001**, *42*, 4367−4373.
(44) Wenger, M.; Armbruster, T. Crystal Chemistry of Lithium: Oxygen Coordination and Bonding. *Eur. J. Mineral.* **1991**, *3*, 387−400.
(45) Johansson, P.; Tegenfeldt, J.; Lindgren, J. Modelling Lithium Ion Transport in Helical PEO by Ab Initio Calculations. *Polymer* **2001**, *42*, 6573−6577.
(46) Memboeuf, A.; Vékey, K.; Lendvay, G. Structure and Energetics of Poly(Ethylene Glycol) Cationized by Li^+, Na^+, K^+ and Cs^+: A First-Principles Study. *Eur. J. Mass Spectrom.* **2011**, *17*, 33−46.
(47) Mohan, V. M.; Bhargav, P. B.; Raja, V.; Sharma, A. K.; Narasimha Rao, V. V. R. Optical and Electrical Properties of Pure and Doped PEO Polymer Electrolyte Films. *Soft Mater.* **2007**, *5*, 33−46.
(48) Chapi, S.; Raghu, S.; Subramanya, K.; Archana, K.; Mini, V.; Devendrappa, H. Conductivity and Optical Band Gaps of Poly-ethylene Oxide Doped with Li_2SO_4 Salt. *AIP Conference Proceedings*, 2014; Vol. *1591*, pp 1275−1277.
(49) Kumar, B.; Rodrigues, S. J.; Koka, S. The crystalline to Amorphous Transition in PEO-based Composite Electrolytes: Role of Lithium Salts. *Electrochim. Acta* **2002**, *47*, 4125−4131.
(50) Mannodi-Kanakkithodi, A.; Huan, T. D.; Ramprasad, R. Mining Materials Design Rules from Data: The Example of Polymer Dielectrics. *Chem. Mater.* **2017**, *29*, 9001−9010.
(51) Sendek, A. D.; Yang, Q.; Cubuk, E. D.; Duerloo, K.-A. N.; Cui, Y.; Reed, E. J. Holistic computational structure screening of more than 12 000 candidates for solid lithium-ion conductor materials. *Energy Environ. Sci.* **2017**, *10*, 306−320.
(52) Mannodi-Kanakkithodi, A.; Chandrasekaran, A.; Kim, C.; Huan, T. D.; Pilania, G.; Botu, V.; Ramprasad, R. Scoping the Polymer Genome: A Roadmap for Rational Polymer Dielectrics Design and Beyond. *Mater. Today* **2017**, *21*, 785−796.
(53) Botu, V.; Batra, R.; Chapman, J.; Ramprasad, R. Machine Learning Force Fields: Construction, Validation, and Outlook. *J. Phys. Chem. C* **2016**, *121*, 511−522.
(54) Botu, V.; Chapman, J.; Ramprasad, R. A study of adatom ripening on an Al (1 1 1) surface with machine learning force fields. *Comput. Mater. Sci.* **2017**, *129*, 332−335.
(55) Ramprasad, R.; Batra, R.; Pilania, G.; Mannodi-Kanakkithodi, A.; Kim, C. Machine Learning in Materials Informatics: Recent Applications and Prospects. *npj Comput. Mater.* **2017**, *3*, 54.
(56) Huan, T. D.; Batra, R.; Chapman, J.; Krishnan, S.; Chen, L.; Ramprasad, R. A Universal Strategy for the Creation of Machine Learning-based Atomistic Force Fields. *npj Comput. Mater.* **2017**, *3*, 37.
(57) Kim, C.; Chandrasekaran, A.; Huan, T. D.; Das, D.; Ramprasad, R. Polymer Genome: A Data-Powered Polymer Informatics Platform for Property Predictions. *J. Phys. Chem. C* **2018**, *122*, 17575−17585.

DOI: 10.1021/acs.chemmater.8b03434
Chem. Mater. 2018, 30, 8804−8810